Egyptian Journal of Chemistry
http://ejchem.journals.ekb.eg/

Novel Schiff Bases Ligands and Their Complexes: Thermal Analysis Antibacterial Activity, and Molecular Docking

Basher J. Kadhem[a], Jassim Alshawi[a], Tahseen A. Alsalim[a]* and Mohnad Abdalla[b]*

aDepartment of Chemistry, Faculty of Education for Pure Sciences, University of Basrah, Basrah, 61001, Iraq
bKey Laboratory of Chemical Biology (Ministry of Education), Department of Pharmaceutics, School of Pharmaceutical Sciences, Cheeloo College of Medicine, Shandong University, 44 Cultural West Road, Shandong Province 250012, PR China

Abstract

The transition metal complexes of novel tetradentate-ketoenamine ligands were synthesised by condensing β-diketone (acetylacetone, 3-chloro acetylacetone) with 4,4'-methylenedianiline. Fourier-transform infrared (FTIR) spectroscopy, proton nuclear magnetic resonance (^{1}H NMR) spectroscopy, carbon-13 NMR (^{13}C NMR) spectroscopy, electron ionisation mass spectrometry (EIMS), elemental analysis, and UV-visible (UV-Vis) spectroscopy were used to describe the compounds while thermogravimetric (TG/DTG) analysis was used to investigate the thermal breakdown of the complexes. All of the complexes showed outstanding stability as well as different degrees of thermal decomposition. Antibacterial activity was tested using gram-positive (Bacillus subtilis, Staphylococcus aureus) and gram-negative (Bacillus subtilis, Staphylococcus aureus) bacteria (Escherichia coli, Salmonella typhi). Minimal inhibitory concentrations (MICs) of 0.5 to 2 mM/ml and minimum bacterial concentrations (MBCs) of 2 to 4 mM/ml were used in this study. A molecular docking study was also conducted to ensure that the compounds connected well to the active sites of the target enzymes; such as topoisomerase II DNA gyrase enzymes (2XCT) and methicillin-resistant Staphylococcus aureus (MRSA,2x3f.pdb).

Keywords: tetradentate, β-diketone, 4,4'-methylene dianiline, β-ketoenamine, Schiff base, antibacterial, acetylacetone.

1. Introduction

Schiff base ligands are formed by a reaction between an aldehyde or ketone and a primary amine; this is one of the oldest known reactions [1]. Tetradentate β-ketoenamine Schiff base ligands that have been produced via the condensation of β-diketone with diamine or monoamine contain N_2O_2 donor atoms [2-11]. Moreover, polydentate and macrocycle Schiff base ligands that have various donor atoms; such asN_2S_2, N_2O_2, N_4,and N_2O [12-14] ;are known to cooperatewell with a variety of metal ions [15-18].
A wealth of articles that extend from pure synthesis to contemporary physically- and biochemically-relevant investigations indicate that the metal complexes of β-ketoenamine ligands have played an essential role incoordination chemistry-based studies [19-25]. Furthermore, the broad-ranging biological and pharmacological consequence of diverse Schiff base metal complexes has piqued the curiosity of researchers [26-30]. Transition metal complexes are most commonly used in the medical field to test antibacterial and anticancer medications in the hopes of developing a feasible and safe treatment for bacterial interactions and cancer [31-33].
As such, this study investigated the synthesis and characterisation of various ketoenamine Schiff bases. Tetradentate ligands were obtained via the condensation of acetylacetone and 3-chloro

*Corresponding author e-mail:. tahseen.alsalim@uobasrah.edu.iq (T.A.alsalim) Tel.: +9647710822163., Mohnad Abdalla, mohnadabdalla200@gmail.com , (M. Abdalla)
Receive Date: 26 September 2021, Revise Date: 08 December 2021
Accept Date: 12 December 2021, First Publish Date: 12 December 2021
DOI: 10.21608/EJCHEM.2021.95037.4571

acetylacetone with 4,4'-methylenedianiline. Transition metal ions; such as Fe^{+3}, Cu^{+2}, Co^{+2}, Cr^{+3} and vanadyl (VO^{2+}); were then used to coordinate the ligands.

2. Material and methods

2.1. Instrumentation and spectral measurements

In the KBr pellet method, FTIR spectra were acquired using a Shimadzu® FTIR-Affinity-1 spectrophotometer in the 4000 to 400 cm^{-1} range. An Agilent Technologies® 5975C spectrometer was then used to scan the mass spectra according to the estimated index (EI)method at 70 eV. The ^{1}H and ^{13}C NMR spectra of the compounds were scanned using a Bruker® 500 MHz spectrometer. Tetramethylsilane (TMS) was utilised as a reference for internal standards. Dimethyl sulfoxide-d_6 (DMSO d_6) was used as the solvent. Melting points were measured on an electrothermal instrument. A PG Instruments® T80+ UV/Vis spectrophotometer was used to measure absorption and reflectance in the UV–vis spectral region. A magnetic susceptibility balance (MSBMkI) was used to record complicated magnetic susceptibility. A Buck Scientific ® 210VGP atomic absorption spectrophotometer was used to measure the metal content of the complexes. A Mettler Toledo® was used to conduct TGA analysis to determine the coordinated water or crystal water while an Elementar® vario MICRO cube CHNS elemental analyser was used for elemental analysis. BioTek® STAT FAX 2100 Microplate Reader

2.2. Chemistry section

Condensation of β–diketone with 4,4'-methylene dianiline yielded two forms of tetradentate-β ketoenamine ligands.

2.2.1. Synthesis of β-ketoenamine Ligands in General (H2L1, H2L2)

β-diketone (acetylacetone, 3-chloro acetylacetone) 0.04 mol was added to a solution of 4,4'-methylene dianiline (0.02mol, 3.96 g) in 40ml ethanol. The reaction mixture was heated under reflux for four hours. The solid product was then collected and recrystallised from ethanol.

2.2.1.1.(Z,2'Z,4E,4'E)-4,4'-((methylenebis(4,1-phenylene))bis(azanylylidene))bis(pent-2-en-2-ol) ;(H_2L1)

Yellow Powder, recrystallized from ethanol:ether (8:2), yield:82% ,M.P: 104-105°C, ^{1}HNMR (DMSO-d_6, δppm) 12.44(s,2H,OH), 7.11(d,4H, *J*=7, ArH), 7.23(d,4H, *J*=7, ArH), 5.21 (s,2H,-C=CH) ,3.92 (s, 2H, Ph-CH_2-Ph),1.98 (s,12H ,CH_3). ^{13}C NMR , 194.9 , 159.8, 138.1, 137.4, 136.4, 129.49, 129.44, 124, 123.7, 97.4, 28.9, 19.4 ; EI- Mass (70ev m/z) : 362. 345, 319 ,305, 279, 208 ,188,44. IR(υ,cm^{-1})3070, 2910, 1622, 1589, 1560, 1283. UV(nm): 216 (ε= 10807.5) ,232 (ε=4700), 321 (λ_{max}12238).

2.2.1.2.(E,2'E,4E,4'E)-4,4'-((methylenebis(4,1-phenylene))bis (azanylylidene))bis (3-chloropent-2-en-2-ol , (H_2L2);
Beige crystallized recrystallized from ether yied:90% ,M.P: 128-126 °C, ^{1}HNMR (DMSO, δppm), 12.72 (s,2H,OH),7.27(d, 4H, *J*=7, ArH), 7.14 (d,4H, *J*=7, ArH), 3.96 (s, 2H, Ph-CH_2-Ph), 2.26 (s, 6H,CH_3=C-OH), 2.15 (s, 6H, CH_3-C=N) , ^{13}C NMR: 193, 158.9, 139, 135.9, 129.9, 129.4, 128.9, 125, 103.3, 28.3, 18, EI- Mass(70ev m/z) : 30.396, 208, 222, 186, 130, 144,90. IR(υ,cm^{-1}) 3057,1977, 1637,1600, 1436, 1209. UV(nm): 216 (ε =8900), 235.6 (ε = 6484.5) ,338.6 (ε =13969.5).

2.2.2. Synthesis of Transition Metal Complexes in General

A 0.01 mol Schiff base ligand solution and a solvent with a ratio of 4:6:6 of dimethylformamide, ethanol, methanol (DMF:EtOH:MeOH) was treated with a 0.02 mol metal salt solution in the same solvent. The mixed reaction was then heated under reflux for five hours. The complex product was recovered via filtration and washed with EtOH and Et2O three times before it was vacuum dried.

2.2.2.1. Complex [Cu (L_1 .$2H_2O$):
Brown powder ,yield 70% ; M.P.>200 °C; IR(υ,cm^{-1}) :3342,3030,2914,1564, 1512, 1201; UV-Visb, λ_{max} (ε) :366nm (6725.5), 304nm (5840.8), 476nm (519.2) , 633nm (43.2); Molar conductance (Ω^{-1} .cm^2 .mol^{-1}) : 2.2 ; μ_{eff} (B.M.) :1.7 ; Elemental analysis (C_{23} H_{28} CuN_2O_4); calculated: M,13.81; C, 60.05; H, 6.13; N, 6.9, found: M,13.24 ; C, 59.82; H, 6.10; N, 6.37.

2.2.2.2. Complex [Co (L_1.$2H_2O$)]$2H_2O$:
Olive powder ; yield 75% ; M.P.>200°C; IR(υ,cm^{-1}) :3354,3032,2937,1608, 1546, 1522,1217; UV-Visb, λ_{max} (ε) :361 nm (10452), 369 nm (10341), 613.9 nm (240), 679 nm (40) ; molar conductance (Ω^{-1}.cm^2. mol^{-1}):11 ; μ_{eff} (B.M.):4.43; Elemental analysis ($C_{23}H_{32}CoN_2O_6$) ;calculated:M,11.99; C, 56.31; H, 6.56 ; N, 6.15; found: M, 11.55 ; C, 56.13; H, 6.43; N,6.42.

2.2.2.3. Complex[Cr (L_1.Cl.H_2O)]H_2O

Umber powder ; yield 65% ; M.P.>200°C; IR(υ,cm^{-1}) :3358,3061,2877,1554,1527, 1517 ,1203; UV-Visb $\lambda_{max}(\varepsilon)$:298nm(6331), 334nm (7100), 642nm (52.9), 679nm; molar conductance ($\Omega^{-1}.cm^2.\ mol^{-1}$): 16.5 ; μ_{eff} (B.M.) :3.8; Elemental analysis ($C_{23}H_{28}ClCrN_2O_4$) ; calculated: M,10.74; C, 57.08; H, 5.83; N, 5.39; found: M, 10.2 ; C, 56.91; H, 5.98; N, 5.39.

2.2.2.4. Complex[Fe (L_1.Cl.H_2O)]H_2O
Brown powder ;yield 75% ;M.P.>200 °C; IR(υ,cm^{-1}) :3319,3012,2964,1666, 1600, 1527,1205; UV-Visb, $\lambda_{max}(\varepsilon)$:268.2nm (7004.4),464nm (nm106.33), 629 nm(85.2); molar conductance ($\Omega^{-1}.cm^2.\ mol^{-1}$): 11; μ_{eff} (B.M.):5.9; Elemental analysis ($C_{23}H_{28}ClFeN_2O_4$); calculated: M,11.45 C, 56.63; H, 5.79; N, 5,74 , found: M,10.89 ; C, 56.44; H, 5.81; N, 5.41.

2.2.2.5. Complex[VO(L_1.H_2O)]H_2O
Dark green powder ; yield 80% ; M.P.>200 °C; IR(υ,cm^{-1}) :3313 ,2910,1651,1608, 1510, 1120; UV-Visb, $\lambda_{max}(\varepsilon)$:263nm (7004.4),420nm (388.8) ,615 (nm 78.2), molar conductance ($\Omega^{-1}.cm^2.\ mol^{-1}$) :15.5; μ_{eff} (B.M.):1.5 ; Elemental analysis ($C_{23}H_{28}N_2O_5V$); calculated: M, 10.99 ; 59.61 ; C, 59.61; H, 6.09; N,6.04 , found: M,10.37 ; C, 59.39; H, 6.21; N, 6.29.

2.2.2.6. Complex[Cu(L_2.$2H_2O$)]
Brown powder ; yield 75% ; M.P.>200 °C; IR(υ,cm^{-1}) :3319,3034,2925,1672,1627, 1598,1236; UV-Visb, $\lambda_{max}(\varepsilon)$:269.8nm(7241.6),422nm (624.4),581nm(160); molar conductance ($\Omega^{-1}.cm^2.\ mol^{-1}$):11; μ_{eff} (B.M.):1.91; Elemental analysis ($C_{23}H_{26}ClCuN_2O_4$) ; calculated : M,12.01; C, 52.23; H, 4.95; N, 5.30; found: M, 12.34 ; C, 51.81; H, 4.81; N,5.45.

2.2.2.7. Complex [Co(L_2.$2H_2O$)]
Dark green powder ; yield 70% ; M.P.>200 °C,IR(υ,cm^{-1}) :3350, 3059, 2972, 1649, 1600, 1510, 1112; UV-Visb, $\lambda_{max}(\varepsilon)$:304nm (8579.2), 478nm(922.5),610nm (91.46),628nm (82.47); molar conductance ($\Omega^{-1}.cm^2.\ mol^{-1}$):16.5; μ_{eff} (B.M.) :4.63; ($C_{23}H_{26}ClCoN_2O_4$); calculated: M,11.24; C, 52.69; H, 5.00; N, 5.34; found: M, 11.02 ; C, 52.47; H, 5.16; N, 5.07.

2.2.2.8. Complex [Cr L_2.Cl.H_2O]H_2O
Brown powder; yield 76% ; M.P.>200 °C; IR(υ,cm^{-1}) :3367,3037, 2966,1656,1600, 1560, 1047.UV-Visb, $\lambda_{max}(\varepsilon)$:267nm (8499.6), 340nm (2464.2), 445nm (238.9), 601nm (80.2) ; molar conductance ($\Omega^{-1}.cm^2.\ mol^{-1}$):22; μ_{eff} (B.M.):3.7.;Elemental analysis ($C_{23}H_{26}Cl_3CrN_2O_4$); calculated: M,9.41, C, 49.97; H, 4.74; N, 5.07; found: M,9.18; C, 49.58; H, 4.58; N, 5.23.

2.2.2.9. Complex [Fe (L_2.Cl.H_2O)]$2H_2O$
Umber powder ; yield 73% ,M.P.>200°C,IR(υ,cm^{-1}) :3336, 3008, 2964, 1651, 1593, 1508; 1174.UV-Visb, $\lambda_{max}(\varepsilon)$: ++-275nm (7476), 324nm (5960), 450nm (633.2),625nm (142.5); molar conductance ($\Omega^{-1}.cm^2.\ mol^{-1}$):14.3; μ_{eff} (B.M.) :5.88 ; Elemental analysis ($C_{23}H_{28}Cl_3FeN_2O_5$);calculated: M , 9.72, C, 48.07; H, 4.91; N, 4.87; found: M,9.72; C, 48.32; H, 4.85; N, 4.51.

2.2.2.10. Complex[VO (L_2.H_2O)]
Olive powder ; yield 80% ; M.P.>200 °C; IR(υ,cm^{-1}) :3253, 3035, 2918, 1670, 1600, 1514, 1118; UV-Visb, $\lambda_{max}(\varepsilon)$:284nm (7237.8), 463nm(724.2),637 (nm 184.4); molar conductance ($\Omega^{-1}.cm^2.\ mol^{-1}$):13.2; μ_{eff} (B.M.) :1.7; Elemental analysis ($C_{23}H_{24}Cl_2N_2O_4V$);calculated: M,9.91; C, 53.71; H, 4.70; N, 5.45; found: M, 9.61; C,53.18; H,4.78; N, 5.20.

2.3. Antibacterial Assay

2.3.1. Bacterial strains

In vitro tests were performed to investigate the antibacterial activity of the produced Schiff base ligands and metal complexes. The antibacterial activity was tested against a variety of Gram-positive and Gram-negative bacteria species; such as Staphylococcus aureus, Enterococcus, Escherichia coli, and Salmonella typhifaecalis; using a modified Kirby-Bauer disc diffusion method [21].

2.3.2. Bacterial Cultures [34]

The broth microdilution method was used to determine the minimum inhibitory concentrations (MICs). The MICs were calculated as the lowest concentrations of each tested chemical that was required to prevent observable bacterial growth. This was accomplished by following the standard protocols as suggested by the Clinical Laboratory Standard Institute (CLSI).
Two-fold serial dilutions of each chemical were made, with concentrations ranging between 0.003 to 4 mM, in sterile plastic micro-dilution trays of Mueller Hinton broth medium. Bacterial suspensions of each bacterial strain were then generated using newly grown cells in normal saline that had been adjusted to a McFarland standard turbidity of 0.5. Prior to transferring the solution to trays with varying quantities of each component, it was further diluted (1:100) in sterile Mueller-Hinton broth (MHB). As such, 0.5 to 1106 bacterial cells were evaluated for each chemical concentration.
A total of 96well plates were incubated for 24 hours at 37°C. Resazurin was used as a growth indicator. Each well was filled with 4 l of each 4-mg/ml reagent stock solution in sterile deionised water. A rosy colour indicated bacteria proliferation in the wells. The minimum bactericidal concentrations (MBCs) were calculated using the lowest dosages of each chemical that could kill 99.99 percent of the tested

bacterial cells. MBCs were determined by growing 100 l of no-growth wells from the MIC testing on nutrient agar plates at 37°C for 24 hours before recording the MBC values. Chloramphenicol was utilised as a standard antibiotic. All experiments were performed in triplicate.

2.4. Molecular Docking study

This study used topoisomerase II DNA gyrase enzymes (2XCT.pdb) and methicillin-resistant Staphylococcus aureus (MRSA) (2x3f.pdb)[35, 36] because they are one of the strategies of treating antibiotic-resistant bacteria by inducing an antibacterial medication response. A docking study was conducted to investigate how the ligands interacted with the targeted proteins. Co-crystallised 2XCT.pdb and 2x3f.pdb crystal structures were retrieved for the docking study. Docking is a powerful computational method of predicting the location of a ligand within a protein's active site as well as showing the amino acids that interact with it.
This information helps determine the position of a drug within the active site as well as the coordination between the various interacting groups.
AutoDock® Vina was used to run docking simulations and calculate the free binding energy between the ligand and the protein. BIOVIA®2020 Discovery Studio Suite and ChemOffice®2015 were used for additional molecular modelling applications. Only one chain and its co-crystallised ligand were retained after the water molecules had been removed from the protein's surface. The hydrogen atoms were then concealed and the protein structure was protonated in three dimensions. The binding pocket of the protein was then determined. The synthesised compounds and co-crystallised ligand were docked using a conventional method. Genetic algorithm searches were used to generate several docked structures in each case. Locations with the best scores were evaluated visually.

3. Results and discussion

The H_2L1 and H_2L2 Schiff base ligands were prepared via direct condensation of 4,4'-methylene dianiline with appropriate β-diketone (acetylacetone or 3-chloro acetylacetone) in the presence of glacial acetic acid (Scheme 1). Transition metal complexes (Figure1)were synthesised from reactions between Schiff base ligands and various transition metals salts; such as $CuCl_2.2H_2O$, $CoCl_2.6H_2O$, $CrCl_3$, $FeCl_3$, $VOSO_4.5H_2O$); in a 4:6:6 ratio of DMF:EtOH:MeOH solvent under reflux. The presence or absence of free ligand was efficiently monitored using thin layer chromatography (TLC) with EtOH:$CHCl_3$ (2:8 v/v) as the eluent. The absence of free ligand indicates complete conversion.

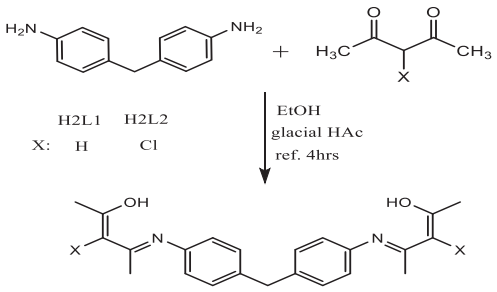

Scheme 1. Synthesis pathway of ligand H_2L1 and H_2L2

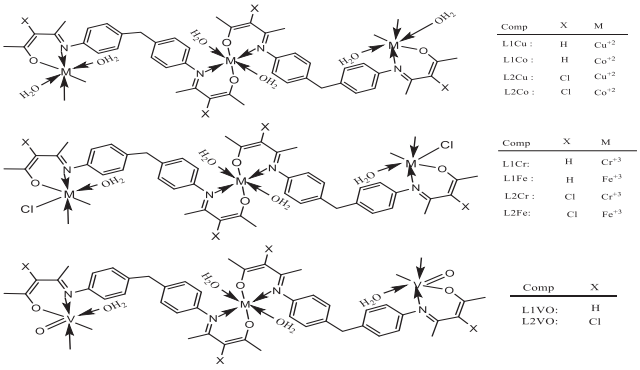

Figure 1. Suggested structure of metal complexes

3.1. Characterization of Ligands and complexes

Multiple types of spectroscopies were used to characterise the synthesised compounds. FTIR spectroscopy of the ligands indicated a strong band of stretching vibration within the υ range of 1622 to 1637 cm^{-1}, which is attributed to C=N. This indicated the formation of enamine from the condensation of the carbonyl group with an amino group. The C=O band of another carbonyl group was not observed because of conversion to the enol form. Also noted were stretching vibration of the C=C of aromatic rings between 1589 to 1600cm^{-1} and bending vibration bands of C-N and C-O at 1560 to 1512 $cm^{-1}$and 1209 to 1238 cm^{-1}, respectively.
The IR spectra of the complexes showed a broadband between 3392 to 3454 cm^{-1} due to the water from coordination and crystallisation. The ^{1}HNMR spectrum of H_2L1 (Figure 2) indicated a singlet signal of CH_3 at δ of 1.89 ppm. The singlet signal at δ of 3.92 was attributed to the methylene group between the aromatic rings, and the singlet signal at δ of 5.21 was the CH=C. Doublet signals of aromatic protons occurred at υ of 7.11 (*J*=7) and 7.23 (*J*=7) while an OH signal of enol formed at 12.44 ppm. This signal confirmed the conversion to enol.

The ^{1}HNMR spectrum of H_2L2 (Figure 3) displayed the same signals with the absence of the CH=C signal due to the chloride atom.

The ^{13}CNMR spectrum of the two ligands indicated that the signal for C=N was between 194.9 to 198ppm and C-OH at 159.38 to 158.5 ppm for H_2L1 and H_2L2, respectively. Signals for the other carbon atoms were also noted.

Mass spectrometry was used to validate the molecular ion peaks of the Schiff base ligands as well as study the fragment species. This is a strong structural characterisation method in coordination chemistry. The fragment pattern of the mass spectrum implied that the target molecule was decaying in stages, with a series of peaks corresponding to the various fragments. Additionally, the mass spectrum results agreed with the proposed formula of the ligands. This molecular formula was determined via elemental analysis of the complexes. Differences between the elemental percentages of the measured and calculated formulas were always within permissible limits.

4. Thermal analysis

A thermal analysis (TG/DTG) of the Schiff base complexes was performed to determine the thermal st ability of the new complexes as well as the condition of water molecules within a nd outside the inner coordination sphere of the core metal ion[37]. The complexes were evaluated at TG in a nitrogen atmosphere up to 600°C with a heating rate of 10°C/min. The losses in mass caused by the TG curves matched the estimated values very well. Table 1 summarises the results of the thermal investigation of the complexes.

The expected structures were confirmed by the breakdown paths of all the complexes. There were two steps in the breakdown of the CuL1 complex. The first phase was accompanied by weight loss at 100 to 200°C (observed = 8%, calculated = 7.85%), which was attributed to the loss of two coordinated water molecules. The ligand broke down in the following stage and the residual product at 600ºC resulted in a 28% weight loss. The remaining 63%was the surviving portions of the ligand at the end of the phase, which was higher than the percentage of CuO (14.13% theoretically). This indicated that the compound was thermally stable.

In the disintegration steps of the other complexes, rapprochement was discovered. Decomposition of the CoL1 complex occurred in three stages. At 80 to 100ºC, the first step was accompanied by weight loss (observed= 8%, calculated= 7.9%). This indicated the loss of two lattice water molecules. An 8% decrease in weight occurred in the second phase (theoretically 7.9%), which was due to the loss of two coordination water molecules. The final phase depicted the loss of sections of the ligand throughout temperatures of100 oC 200 to 600°C, with a loss rate of 34.15%. The remaining 49.85% revealed a close to 50% loss of the molecule, which was more than the proportion of cobalt oxide (CoO) present (calculated= 14.94%). This finding demonstrated the stability of the complex.

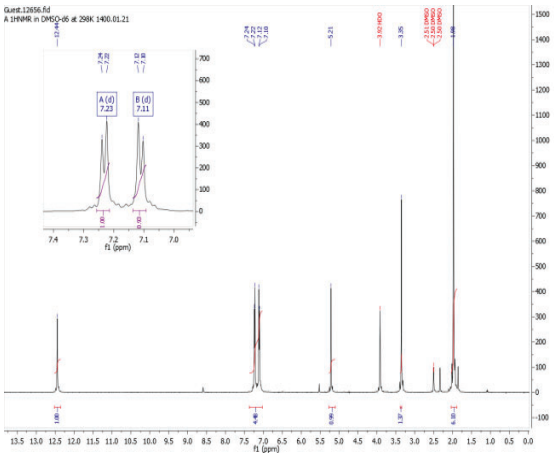

Figure 2. ^{1}HNMR spectrum of compound H_2L1

The Decomposition of the CrL1 and FeL1 complexes occurred in four stages. The lattice water molecules of CrL1 and FeL1 (observed=4%, calculated=3.87%; observed=4%, calculated=3.835%, respectively) occurred in the initial step of weight loss. Weight loss of a coordination water molecule and hydrochloride molecules occurred during the second step of the breakdown. With the loss of sections of the ligand, the third and fourth stages are depicted in the TG diagram. The VOL1 complex underwent four steps of decomposition. The loss of a lattice water molecule occurred in the first step of decomposition (observed=3.8 %, calculated=3.88 %). The second phase was performed at 105 to 170°C (DTG max 150ºC). The loss of two coordination water molecules caused the weight loss from the breakdown (observed=3.8 %, calculated=3.88 %). Parts of the ligand were lost at 170 to 600ºC in the third and fourth phases. The 35.25% weight reduction plus the remaining 57.15% weight loss were nearly equal to a 50% compound loss. This demonstrated the stability of the complex.

As indicated in Table 1, ligand 2 complexes (CuL2, CoL2, CrL2, FeL2, and VOL2) exhibited similar breakdown stages to that of ligand 1 complexes. The

CuL2 complex decomposed in two phases. The initial step of decomposition was accompanied by weight loss (observed = 7%, calculated = 6.8%), which was attributed to the loss of two coordinated water molecules at 100 to 190ºC. The ligand and residual product then decomposed at 600°C, resulting in weight losses of 38.7% and 54.30%, respectively. This suggested that portions of the ligand survived due to stability.

Decomposition of the CoL2 complex occurred in three stages. At 100 to 180°C, the initial breakdown phase was accompanied by weight loss (observed = 7%, calculated = 6.87%), which was attributed to the loss of two coordination water molecules. The weight loss of sections of the ligand was seen in the second and third phases, which extended to temperatures of 180 to 600°C with a loss of 44.93%with 48.07% remaining. At 221 to 600°C, the TGA curve of the CrL2 complex showed three stages of mass loss, the first of which (observed = 4%, calculated = 3.87%) corresponded to the release of one lattice water molecule.

One coordination water molecule and one HCl molecule were lost in the second breakdown stage at 105 to 221°C (observed = 11.36%, calculated = 11.60). The TG and DTG curves at 221 to 600°C indicated the third and fourth phases. They demonstrated that components of the ligand were lost, with a weight loss of 40.59% and 45.15% of the remaining ligand. This indicated that components of the ligand survived

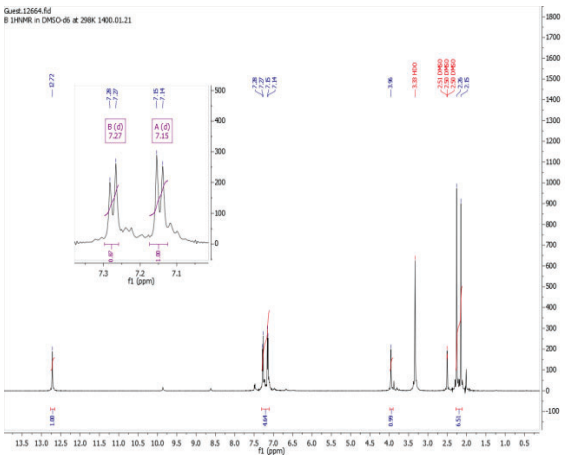

Figure 3. ^{1}H NMR spectrum of compound H_2L2

The TG curves of the FeL2 complexes indicated four breakdown phases. Weight loss (observed = 6.6%, calculated = 6.69%) was recorded at 25 to 125ºC due to the loss of two lattice water molecules. The complex lost a coordination water molecule and a hydrochloride molecule in the second stage, thereby losing 10.1% of its weight (calculated = 10.2%). The loss of sections of the ligand (27.17%) was represented by weight loss in the third and fourth steps while the remaining weight was 56.13%.The TG and TDG curves of the VOL2 complex showed decomposition. The first step was the loss of the lattice water molecule and, in the second step, the complex lost the coordination water molecules (observed = 3.5%, calculated = 3.38%). The final two steps showed the loss of parts of the ligand. They extended from 205 to 600ºC with a loss rate of 26.84% with 69.66% remaining. The results of the TG/DTG analyses indicated that all the complexes had excellent stability and thermal decomposition at various stages.

5. Kinetic and thermodynamic data analysis

The integrated Coats and Redfern method was used to kinetically analyze the thermal dehydration and decomposition of the complexes [38]. The activation energy (E), frequency factor (A), enthalpy of activation (H), the entropy of activation (S), and Gibbs free energy change of the breakdown (G) of the hydrated complexes were graphed using the TG and DTG data.

$$\log\left[\frac{\log\frac{W_f}{W_f - W_t}}{T^2}\right] = \log\left[\frac{AR}{\theta E}\left(1-\frac{2RT}{E}\right)\right] - \frac{E}{2.303\,RT}$$

Where W_f is the weight loss at the end of the stage; W_t is the weight loss at temperatures t; E, R, A, and X are the activation energies; and R is the gas constant.

Negative entropy values indicate that the entire process is occurring at a slow pace. It also shows that the activated compound is more ordered than either of the reactants [39, 40]. The H of all the complexes were positive, indicating that the reaction was endothermic. Furthermore, all the G values were positive, indicating that none of the steps were random. Table 2 presents the thermo-kinetic data.

6. Electronic spectra

The electronic spectra of the H_2L1 ligand showed two absorption bands at wavelengths of 225nm (ε=10807mol^{-1}.cm^{-1}) and 326nm (ε=12238 mol^{-1}. cm^{-1}) due to π–π* [41, 42]. The spectra of the H_2L2 ligand displayed two absorption bands at 240 nm (ε

=6484 $mol^{-1}.cm^{-1}$) and 338nm (ε=14969 $mol^{-1}.cm^{-1}$), which were also due to π–π*. The electronic spectra of all complexes had absorption bands in the 225 to 375 nm region (ε= 12579 to 6484 $mol^{-1}.cm^{-1}$), which was attributed to π–π*.Weak absorption bands of charge transfer were present in the spectra of CuL1, VoL1, CuL2, CoL2, CrL2, FeL2, and VOL2in the visible region at 476 nm (ε =519 $mol^{-1}.cm^{-1}$), 420 nm (ε =388 $mol^{-1}. cm^{-1}$), 422 nm (ε =624 $mol^{-1}.cm^{-1}$), 478 nm (ε =922 $mol^{-1}. cm^{-1}$), 445 nm (ε =238 $mol^{-1}. cm^{-1}$), 450 nm (ε =633 $mol^{-1}.cm^{-1}$), and 463 nm (ε =724 $mol^{-1}. cm^{-1}$), respectively[43, 44]. There were also d-d transition bands in the visible region, with CuL1 and CuL2 showing bands at 633nm and 518 nm, respectively. These were assigned to $^2E_g \rightarrow {}^2T_{2g}$, which agreed with the magnet moments of 1.91 and 1.7 B.M. due to the single electron in the outer orbital [45-47].

The spectra of the CoL1 and CoL2 complexes displayed two weak bands of d-d transition. The first band was from 613 nm (ε= 240$mol^{-1}.cm^{-1}$)to 610 nm (ε= 91$mol^{-1}.cm^{-1}$) and was assigned to the $4T_1(f) \rightarrow 4A_1(p)$ transition. These second band was from 679nm(ε= 40 $mol^{-1}.cm^{-1}$) to 628 nm (ε= 82 $mol^{-1}.cm^{-1}$)and assigned to the$^4T_1g(f) \rightarrow {}^4A_2g(f)$ transition of three electrons in the outer orbital [2, 47-49].

The electronic spectra of the CrL1 and CrL2 complexes showed weak bands of d-d transition at 642 nm (ε= 52$mol^{-1}.cm^{-1}$) and 601 nm (ε= 80 $mol^{-1}.cm^{-1}$), which was assigned to the $^4T1g(F) \rightarrow {}^4A_2g$ (F) transition. This agreed with the magnet moments of 8 and 7.3B.M. due to the three electrons in the outer orbital. The electronic spectra of the FeL1 and FeL2 complexes, respectively, displayed weak bands at 629 nm (ε= 85 $mol^{-1}.cm^{-1}$) and 625 nm (ε=142$mol^{-1}.cm^{-1}$) from the d-d transition and were assigned to the $^6A1g \rightarrow {}^4T1g$ transition. The VOL1 and VOl2 complexes had one absorption band of d-d transition at wavelengths of 615 nm (ε= 615$mol^{-1}.cm^{-1}$) and 637 nm (ε=184 $mol^{-1}.cm^{-1}$), respectively, which were assigned to the$^4T_{2g} \rightarrow {}^4A_{2g}$ transition due to one electron in the outer orbital. This agreed with the magnet moments of 1.5 and 1.7 B.M. [50, 51].

7. Antibacterial Activity Evaluation

freshly synthesized compounds were evaluated for in vitro antibacterial activity using chloramphenicol as a control medication. Gram-positive bacteria Bacillus subtilis (PTCC 1023) and Staphylococcus aureus (ATCC 25923) as well as Gram-negative species Escherichia coli (ATCC 25922) and Salmonella typhi (PTCC 1609) were tested. Table 3 shows the inhibitor values of the produced molecules. At doses of 0.003to 4 mM, the newly synthesised chemicals showed antibacterial activity against the test organisms. According to the findings, the antibacterial activity of the produced compounds depended on their chemical structure.

The average MICs of the H_2L1 and H_2L2 substances were the lowest, with MICs between 0.5 to 2 mM (0.5-1 mM). Antibacterial activity was also detected in the remaining compounds. MBCs of 2 to 4 mM were the highest recorded.

8. Results of Molecular Docking Study

Molecular docking of the H_2L1 and H_2L2 chemicals revealed binding sites on the structure of MRSA and 2XCT (Figures 4 to 7 and Table 4). Docking against the MRSA protein indicated a well-conserved binding domain, while estimated optimum binding energy differed marginally. The H_2L2 compound (-7.5 kcal/mol) had the highest free binding energy, while the H_2L1 compound (-6.7 kcal/mol) had the lowest. The H2L2 compound had a free binding energy of -7.7 kcal/mol against 2XCT while the H_2L1 compound had a free binding energy of -7.5 kcal/mol. At the 2X3F pocket, the H_2L1 compound established three hydrogen bonds with the Glu12, Asp143, and Asp143 residues as well as hydrophobic interactions with the Glu12, Ala168, Glu170, Lys16, and Met141 residues (Figure4).It also had one hydrogen bond with the Met1113 residue and hydrophobic interactions with the Leu1110, Asp1096, Gly1106, Ser1112, Asp587, and Met1113 residues in the 2XCT pocket (Figure5). Three hydrogen bonds were formed with the Lys18, Gly37, and Met31 residues by the H2L2 compound with the 2X3F pocket as well as hydrophobic interaction with the His38, Thr30, Met31, Pro29, Lys150, Glu154, and Asp151 residues (Figures 6A& 6B). It also had three interactions with the Asp1096, Phe1480, Thr1129, ala1094, Gly1104, Pro1102, and Gly1106 residues to occupy the 2XCT pocket (Figure 7). Based on this docking analysis, it was predicted that ligands with a high binding affinity for a target protein would have more antibacterial activity. During in vitro examinations, the chemicals demonstrated improved antibacterial activity against all microbes. This data on antibacterial activity corroborated the findings of the docking analysis. These compounds were successfully accommodated at the active site of the enzyme, according to docking scores, and their binding patterns demonstrated that they interacted considerably inside the active site of target proteins.

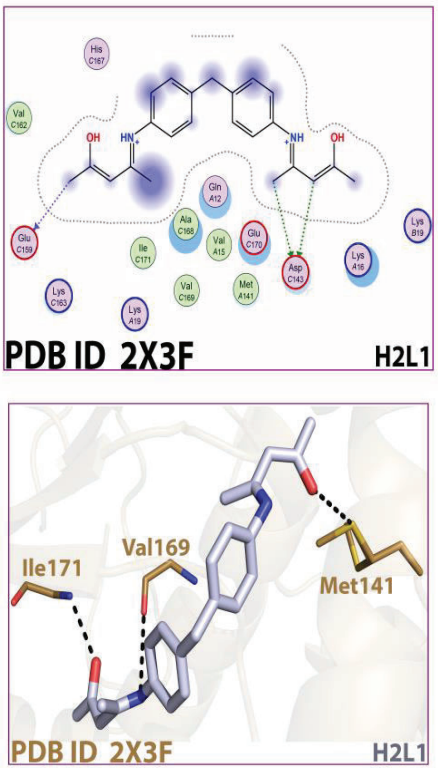

Figure 4. 2D and 3D predicted binding from docking simulation of H2L1 in to the active site of MRSA(2X3F.pdb)

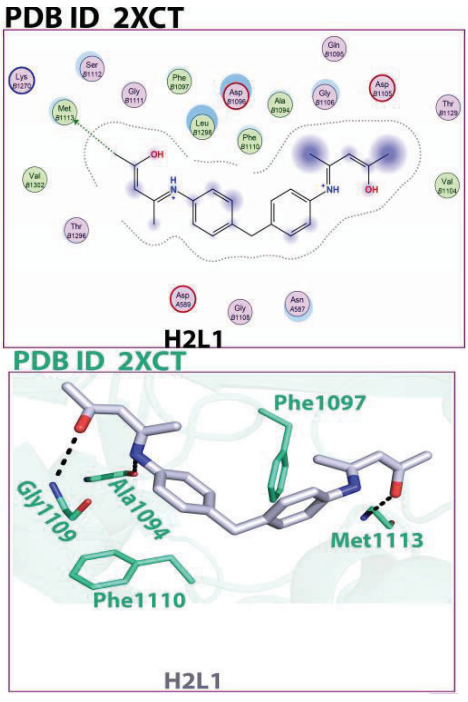

Figure 5. 2D and 3D predicted binding from docking simulation of H_2L1 in to the active site of (2XCT.pdb)

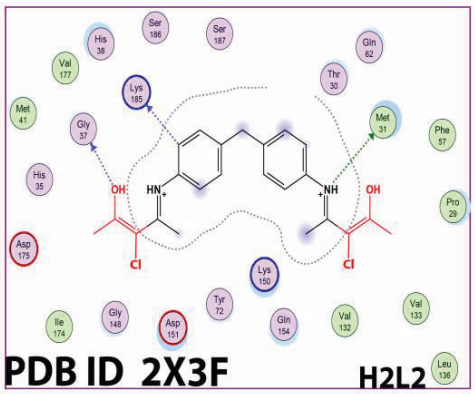

Figure 6. (A) 2D predicted binding mode docking simulation of H_2L2 into the active site of (2X3F.pdb)

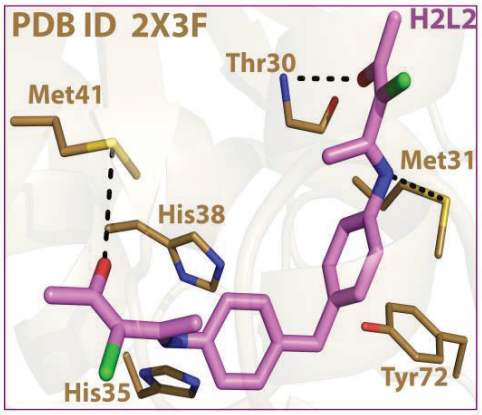

Figure 6. (B) 3D predicted binding mode docking simulation of H2L2 into the active site of (2X3F.pdb)

9. Conclusion

Two ligands and ten transition metal complexes were synthesised. Their antibacterial efficacy was tested against various bacterial species, both gram-positive and gram-negative. The efficacy of the molecule was determined by calculating the MICs and MBCs. The compounds showed good antibacterial activity as well as the molecular docking of the L_2H1 and L_2H2 compounds. In order to observe how ligands interact with the proteins that were studied; 2XCT and 2X3F were successfully accommodated at the active site of the enzyme. According to the docking scores and their binding patterns, they were found to interact considerably within the active site of target proteins. Based on these result and observations, ligands and their complexes may be able to simulate the H_2L2 compound into the active site of the 2X3F.pdb enzyme.

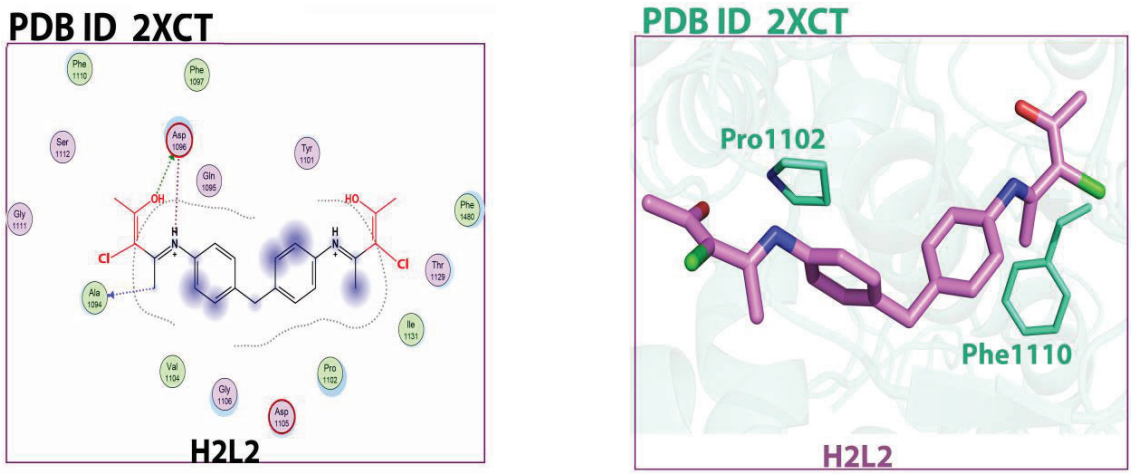

Figure 7. 2D and 3D predicted binding from docking simulation of H2L2 into the active site of (2XCT.pdb)

Table 1. Thermal data of complexes

Complex.	Decomposition Temp.°C			Remaining product at 600 °C	weight Loss% (Calc.)	Assignment
	T_i	T_{op}	T_f			
CuL1	100 200	135	200 600	63%	8(7.85) 28	$2H_2O$, coord
CoL1	25 100 200	70 140	100 200 600	49.85%	8(7.9) 8(7.9) 34.15	$2H_2O$, lattice $2H_2O$, coord
CrL1	25 100 265	75 180	100 265 600	40.21%	4(3.87) 11.36(11.6) 43.79	H_2O, lattice H_2O+HCl, coord
FeL1	25 135 275	125 275	135 275 600	52.26	4(3.83) 11(11.6) 32.74	H_2O, lattice H_2O+HCl
VoL1	25 105 170	75 150	105 170 600	57.15	3.8(3.88) 3.8(3.88) 35.25	H_2O, lattice H_2O, coord
CuL2	100 190	130	190	54.30%	7(6.8) 38.7	$2H_2O$, coord
CoL2	100 180	145	180 600	48.07%	7(6.87) 44.93	$2H_2O$, coord
CrL2	25 105 221	95 140	105 221 600	45.15%	4(3.87) 9.8(9.9) 40.95	H_2O, lattice H_2O+HCl, coord
FeL2	25 125 283	52 136	125 283 600	56.13%	6.6(6.69) 10.1(10.2) 27.17	$2H_2O$, lattice H_2O+HCl, coord
VoL2	100 205	180	205 600	69.66%	3.5(3.38) 26.84	H_2O, coord

Table 2. Kinetic parameters of the complexes determined using the Coats–Redfern equation

Comp.	steps	A(s^{-1})	E ($kJ.mol^{-1}$)	ΔH ($kJ.mol^{-1}$)	ΔS($kJ.mol^{-1}K^{-1}$)	ΔG($kJ.mol^{-1}$)
CuL1	1st	$1.1073x10^{2}$	32.23	28.84	-0.20783	113.63
	2nd	$1.6093x10^{3}$	119.343	115.163	-0.187274	105.36
	3rd	$4.9972x10^{3}$	186.926	181.749	-0.179662	293.677
CoL1	1st	$1.528x10^{6}$	103.74	100.89	-0.12718	144.5127
	2nd	$1.433x10^{3}$	187.02	183.58	-0.186575	260.6
	3rd	$4.6724x10^{2}$	17.48	12.303	-0.19930	136.467
	4th	$2.484x10^{5}$	102.75	96.76	-0.148452	204.09
CrL1	1st	$1.095x10^{3}$	47.5	49.609	-0.187384	109.818
	2nd	$3.6898x10^{11}$	133.85	130.08	0.041326	211.38
	3rd	$2.3804x10^{15}$	202.43	197.25	-0.193861	169.98
	4th	$1.2132x10^{5}$	126.93	121.005	-0.135156	217.367
FeL1	1st	$2.3166x10^{2}$	81.009	77.7	-0.18586	126.688
	2nd	$6.551 x 10^{2}$	33.747	27.31	-0.195199	131.351
	3rd	$3.2384x10^{4}$	39.38	34.203	-0.164081	136.4248
	4th	$3.0125x10^{6}$	123.782	117.85	-0.1276	208.82
VOL1	1st	$9.809x10^{5}$	64.90	62.009	-0.130963	107.58
	2nd	$2.838x10^{10}$	115.08	111.565	-47.2174	131.534
	3rd	1.7384x10	52.627	47.278	-0.226917	193.185
	4th	$1.8734x10^{11}$	173.47	167.47	-0.035993	143.513
CuL2	1st	$1.459x10^{2}$	42.47	39.122	-0.205355	121.88
	2nd	$6.7134x10^{2}$	49.99	45.852	-0.19443	142.678
	3rd	$8.5584x10^{5}$	113.51	108.541	-0.1367	190.287
CoL2	1st	$7.8278x10^{2}$	52.8	49.327	-0.1917	129.4576
	2nd	$5.1875x10^{2}$	67.6966	63.433	-0.19682	164.40
	3rd	$2.5835x10^{2}$	80.23	75.303	-0.20382	196.168
CrL2	1st	$7.7807x10^{4}$	59.09	56.04	-0.15242	112.13
	2nd	$5.4872x10^{4}$	21.07	17.638	-0.156283	82.18
	3rd	$8.3121x10^{3}$	86.96	81.783	-0.19451	202.96
FeL2	1st	$1.074x10^{4}$	18.419	15.719	-0.167845	70.268
	2nd	$1.9565x10^{4}$	31.71	28.278	-0.164852	96.3618
	3rd	$8.6429x10^{4}$	99.56	94.799	-0.15523	183.74
	4th	$1.2427x10^{2}$	74.78	69.396	-0.2109	206.06
VOL2	1st	$1.5196x10^{2}$	45.87	42.148	-0.2059	134.3912
	2nd	$6.305x10^{3}$	78.77	74.424	-0.176225	166.59
	3rd	$2.1566x10^{5}$	113.077	107.8	-0.129323	189.66
	4th	$3.2417x10^{14}$	232.219	226.129	-0.165.42	347.3848

Table 3. MICs and MBCs (mM) of synthesised compounds against Gram-positive and Gram-negative bacterial strains

Compound	*B. subtilis*		*S. aureus*		*E. coli*		*S. typhi*	
	MIC	MBC	MIC	MBC	MIC	MBC	MIC	MBC
H2L1	0.5	>4	1	>4	0.5	>4	1	>4
H2L2	0.5	>4	0.5	>4	0.5	>4	0.5	>4
L1Cu.2H_2O	1	>4	2	>4	2	>4	2	>4
L1Co.2H_2O	1	>4	2	>4	2	>4	2	>4
L1Cr.Cl. H_2O	2	>4	1	2	1	4	0.5	2
L1Fe. Cl. H_2O	2	>4	2	>4	2	>4	2	>4
L1VO. H_2O	2	>4	1	>4	2	>4	2	>4

Compound	*B. subtilis*		*S. aureus*		*E. coli*		*S. typhi*	
	MIC	MBC	MIC	MBC	MIC	MBC	MIC	MBC
L2Cu.2H_2O	2	>4	2	>4	2	4	2	>4
L2Co.2H_2O	1	4	2	2	2	>4	1	>4
L2Cr. Cl. H_2O	2	>4	1	4	1	4	0.5	2
L2Fe. Cl. H_2O	2	>4	2	>4	2	>4	2	>4
L2VO. H_2O	1	>4	2	>4	1	>4	2	2
Chloramphenicol (µg/ml)	4	16	1	8	4	8	16	64

Table 4. Docking results of H_2L1 and H_2L2 compounds with a target protein

Target protein	Compound	Ligand	Binding interaction (Amino acid residue)	Interaction	Distance (A°)	Binding interaction Energy (Kcal/mol)	Affinity energy (Kcal/mol)
2X3F	H2L1	C23 14O	Glu159 (B)	H-donor	3.67	-0.7	-6.7
		C15 14OD1	Asp143(B)	H-donor	4.01	-0.7	
		C16 25OD1	Asp143(B)	H-donor	3.72	-1.1	
	H2L2	C2 4O	Lys18(A)	H-donor	3.14	-0.8	-7.5
		O2 15O	Gly37(A)	H-donor	2.74	-1.5	
		N1 23SD	Met31(A)	H-donor	3.89	-1.3	
2XCT	H2L1	C18 29SD	Met1113 (D)	H-donor	3.67	-0.8	-7.5
	H2L2	C15 25O	Ala1094(D)	H-donor	3.54	-1.1	-7.7
		O1 30OD2	Asp1096(D)	H-donor	2.94	-1.2	
		N1 23OD1	Asp1096(D)	H-donor	3.99	-0.5	

10. Conflicts of interest

There are no conflicts to declare

11. Funding

This work was financially supported by the Authors.

References:

[1] P. Bhowmik, M.G. Drew, S. Chattopadhyay, Synthesis and characterization of nickel (II) and copper (II) complexes with tetradentate Schiff base ligands, Inorganica Chimica Acta 366(1) (2011) 62-67.

[2] S. Chandra, L.K. Gupta, EPR, IR and electronic spectral studies on Mn (II), Co (II), Ni (II) and Cu (II) complexes with a new 22-membered azamacrocyclic [N4] ligand, Spectrochimica Acta Part A: Molecular and Biomolecular Spectroscopy 60(8-9) (2004) 1751-1761.

[3] S. Chattopadhyay, M.S. Ray, M.G. Drew, A. Figuerola, C. Diaz, A. Ghosh, Facile synthesis of Cu (II) complexes of monocondensed N, N, N donor Schiff base ligands: Crystal structure, spectroscopic and magnetic properties, Polyhedron 25(11) (2006) 2241-2253.

[4] J.-P. Costes, F. Dahan, J.M. Dominguez-Vera, J.-P. Laurent, J. Ruiz, J. Sotiropoulos, Stereoisomerism in the Nickel (II) Complexes of a Chiral Tridentate Ligand: Solid-State and Solution Study, Inorganic Chemistry 33(18) (1994) 3908-3913.

[5] J.-P. Costes, M.-I. Fernandez-Garcia, Oxovanadium (IV) complexes of tetradentate unsymmetrical Schiff bases derived from 7-amino-4-methyl-5-aza-3-hepten-2-one, Transition Metal Chemistry 13(2) (1988) 131-134.

[6] P. Ghosh, S.K. Dey, M.H. Ara, K. Karim, A. Islam, A review on synthesis and versatile applications of some selected Schiff bases with their transition metal complexes, Egyptian Journal of Chemistry 62(Special Issue (Part 2) Innovation in Chemistry) (2019) 523-547.

[7] E. Kwiatkowski, M. Klein, G. Romanowski, The optically active and racemic products of monocondensation of 1, 2-diaminopropane and 2, 4-pentadione as ligands and precursors for preparation of unsymmetrical Schiff bases and their nickel (II) complexes, Inorganica chimica acta 293(1) (1999) 115-122.

[8] B. Mabad, P. Cassoux, J.P. Tuchagues, D.N. Hendrickson, Manganese (II) complexes of polydentate Schiff bases. 1. Synthesis, characterization, magnetic properties, and molecular structure, Inorganic Chemistry 25(9) (1986) 1420-1431.

[9] N. Raman, R. Jeyamurugan, B. Rajkapoor, V. Magesh, Metal-based antitumor, cytotoxic and antimicrobial activity: pharmacological evaluation of

Knoevenagel condensate β-diketone Schiff base thiosemicarbazone Cu (II) and Zn (II) complexes, Applied Organometallic Chemistry 23(7) (2009) 283-290.
[10] M. Tümer, Polydentate Schiff-base ligands and their Cd (II) and Cu (II) metal complexes: synthesis, characterization, biological activity and electrochemical properties, Journal of Coordination Chemistry 60(19) (2007) 2051-2065.
[11] Z.-Y. Yang, R.-D. Yang, F.-S. Li, K.-B. Yu, Crystal structure and antitumor activity of some rare earth metal complexes with Schiff base, Polyhedron 19(26-27) (2000) 2599-2604.
[12] A.I. Demehin, M.A. Oladipo, B. Semire, Synthesis, Spectroscopic, Antibacterial and Antioxidant Activities of Pd (Ii) Mixed-Ligand Complexes Containing Tridentate Schiff Bases, Egyptian Journal of Chemistry 62(Special Issue (Part 2) Innovation in Chemistry) (2019) 413-426.
[13] H. Keypour, M. Rezaeivala, Y. Fall, A.A. Dehghani-Firouzabadi, Solvent-free synthesis of some N4O2, N4S2 and N6 Schiff base ligands assisted by microwave irradiation, Arkivoc 10 (2009) 292-301.
[14] W.A. Zoubi, F. Kandil, M. Chebani, Synthesis of macrocyclic schiff bases based on pyridine-2, 6-dicarbohydrazide and their use in metal cations extraction, Organ. Chem. Curr. Res 1(104) (2012) 2161-0401.1000104.
[15] A.A. Abdulkarem, Synthesis and antibacterial studies of metal complexes of Cu (ii), Ni (ii) and Co (ii) with tetradentate ligand, Journal of Biophysical Chemistry 8(02) (2017) 13.
[16] X.R. Bu, E.A. Mintz, X.Z. You, R.X. Wang, Y. Qi, Q.J. Meng, Y.J. Lu, D. Van Derveer, Synthesis and characterization of vanadyl complexes with unsymmetrical bis-schiff base ligands containing a cis-N2O2 coordinate chromophore1, Polyhedron 15(24) (1996) 4585-4591.
[17] S. Chand, M. Tyagi, P. Tyagi, S. Chandra, D. Sharma, Synthesis, characterization, DFT of novel, symmetrical, N/O-donor tetradentate Schiff's base, its Co (II), Ni (II), Cu (II), Zn (II) complexes and their in-vitro human pathogenic antibacterial activity, Egyptian Journal of Chemistry 62(2) (2019) 291-310.
[18] S.-W. Ng, S.-C. Chan, C.-F. Yeung, S.-M. Yiu, C.-Y. Wong, A New Tetradentate Mixed Aza-Thioether Macrocycle and Its Complexation Behavior towards Fe (II), Ni (II) and Cu (II) Ions, Molecules 25(9) (2020) 2030.
[19] T.A. Alsalim, J.S. Hadi, O.N. Ali, H.S. Abbo, S.J. Titinchi, Oxidation of benzoin catalyzed by oxovanadium (IV) schiff base complexes, Chemistry Central Journal 7(1) (2013) 1-8.
[20] M. Attari, M. Mubarak, F. Khalili, Preparation and characterization of some tetradentate Schiff bases and their complexes with Co (II), Ni (II) and Cu (II), Synthesis and Reactivity in Inorganic and Metal-Organic Chemistry 27(1) (1997) 1-16.
[21] A. Bartyzel, Synthesis, crystal structure and characterization of manganese (III) complex containing a tetradentate Schiff base, Journal of Coordination Chemistry 66(24) (2013) 4292-4303.
[22] W.H. Hegazy, Synthesis and structural studies of some β-diketone phenylhydrazones and their complexes with Co (II), Ni (II), and Cu (II), Monatshefte für Chemie/Chemical Monthly 132(5) (2001) 639-650.
[23] N. Margiotta, N. Denora, S. Piccinonna, V. Laquintana, F.M. Lasorsa, M. Franco, G. Natile, Synthesis, characterization, and in vitro evaluation of new coordination complexes of platinum (II) and rhenium (I) with a ligand targeting the translocator protein (TSPO), Dalton Transactions 43(43) (2014) 16252-16264.
[24] M.D. Milton, J.D. Singh, R.J. Butcher, Synthesis of β-ketoenamine donors having O, N, Se/Te donor functionalities and their reaction chemistry with Pd (II) and Pt (II) metal ions, Tetrahedron Letters 45(36) (2004) 6745-6747.
[25] J.-H. Zou, D.-L. Zhu, H. Tian, F.F. Li, F.F. Zhang, G.-W. Yang, Q.-Y. Li, Y.X. Miao, Construction of six new coordination complexes with 5-(3-pyridyl) tetrazole-2-acetato, Inorganica Chimica Acta 423 (2014) 87-94.
[26] U. El-Ayaan, A.-M. Alaa, S. Al-Shihry, Solvatochromism, DNA binding, antitumor activity and molecular modeling study of mixed-ligand copper (II) complexes containing the bulky ligand: bis [N-(p-tolyl) imino] acenaphthene, European journal of medicinal chemistry 42(11-12) (2007) 1325-1333.
[27] W. El-Shwiniy, M.Y. Nassar, A. Shehata, S. El-Desoky, Preparation, characterization, in vitro cell cytotoxicity and biological studies of Pd (II), Ag (I), Pt (IV) and Hg (II) piroxicam anti-inflammatory drug complexes, Egyptian Journal of Chemistry 63(12) (2020) 4671-4680.
[28] A. Matsukage, F. Hirose, M. Yamaguchi, Transcriptional Regulation of DNA Replication–related Genes in Cell Growth, Differentiation and Oncogenesis, Japanese journal of cancer research: Gann 85(1) (1994) 1.
[29] A. Shrivastav, N.K. Singh, S.M. Singh, Synthesis, characterization and antitumor studies of Mn (II), Fe (III), Co (II), Ni (II), Cu (II) and Zn (II) complexes of N-salicyloyl-N′-o-hydroxythiobenzhydrazide, Bioorganic & medicinal chemistry 10(4) (2002) 887-895.
[30] N.K. Singh, A.A. Kumbhar, Y.R. Pokharel, P.N. Yadav, Anticancer potency of copper (II) complexes of thiosemicarbazones, Journal of Inorganic Biochemistry 210 (2020) 111134.
[31] Z.H. Chohan, M. Arif, M.A. Akhtar, C.T. Supuran, Metal-based antibacterial and antifungal

agents: synthesis, characterization, and in vitro biological evaluation of Co (II), Cu (II), Ni (II), and Zn (II) complexes with amino acid-derived compounds, Bioinorganic Chemistry and Applications 2006 (2006).
[32] M. Murugaiyan, S.P. Mani, M.A. Sithique, Zinc (ii) centered biologically active novel N, N, O donor tridentate water-soluble hydrazide-based O-carboxymethyl chitosan Schiff base metal complexes: synthesis and characterisation, New Journal of Chemistry 43(24) (2019) 9540-9554.
[33] M. Shao, X. Liu, Y. Sun, S. Dou, Q. Chen, X.-A. Yuan, L. Tian, Z. Liu, Preparation and the anticancer mechanism of configuration-controlled Fe (ii)–Ir (iii) heteronuclear metal complexes, Dalton Transactions 49(36) (2020) 12599-12609.
[34] J.H. Jorgensen, J.D. Turnidge, Susceptibility test methods: dilution and disk diffusion methods, Manual of clinical microbiology (2015) 1253-1273.
[35] A.-A.S. El-Etrawy, F.F. Sherbiny, Design, synthesis, biological evaluation and molecular modeling investigation of new N'-(2-Thiouracil-5-oyl) hydrazone derivatives as potential anti-breast cancer and anti-bacterial agents, Journal of Molecular Structure 1232 (2021) 129993.
[36] E. Yuanita, I. Sudarma, N. Sudewiningsih, J. Syahri, N. Dharmayani, Sudirman, M. Ulfa, I. Sumarlan, Antibacterial activity and molecular docking studies of series hydroxyxanthone, AIP Conference Proceedings, AIP Publishing LLC, 2020, p. 020032.
[37] R. Ahmadzadeh, M. Azarkish, T. Sedaghat, Synthesis, spectroscopic characterization, thermal analysis and antibacterial activity of Ni (II), Cu (II) and Zn (II) complexes with schiff bases derived from β-Diketones, Journal of the Mexican Chemical Society 58(2) (2014) 173-179.
[38] A.W. Coats, J. Redfern, Kinetic parameters from thermogravimetric data, Nature 201(4914) (1964) 68-69.
[39] H.P. Ebrahimi, J.S. Hadi, Z.A. Abdulnabi, Z. Bolandnazar, Spectroscopic, thermal analysis and DFT computational studies of salen-type Schiff base complexes, Spectrochimica Acta Part A: Molecular and Biomolecular Spectroscopy 117 (2014) 485-492.
[40] A. Frost, R. Pearson, Kinetics and mechanism, The Journal of Physical Chemistry 65(2) (1961) 384-384.
[41] L. John, R.S. Joseyphus, I.H. Joe, Synthesis, spectral characterization, DFT, and molecular docking studies of metal (II) complexes derived from thiophene-2-carboxaldehyde and 2-amino-6-picoline, Journal of Coordination Chemistry 72(16) (2019) 2669-2687.
[42] M.T. Kaczmarek, M. Skrobanska, M. Zabiszak, M. Wałęsa-Chorab, M. Kubicki, R. Jastrzab, Coordination properties of N, N′-bis (5-methylsalicylidene)-2-hydroxy-1, 3-propanediamine with d-and f-electron ions: crystal structure, stability in solution, spectroscopic and spectroelectrochemical studies, RSC advances 8(54) (2018) 30994-31007.
[43] K. Andiappan, A. Sanmugam, E. Deivanayagam, K. Karuppasamy, H.-S. Kim, D. Vikraman, Schiff base rare earth metal complexes: Studies on functional, optical and thermal properties and assessment of antibacterial activity, International journal of biological macromolecules 124 (2019) 403-410.
[44] E.T. Knittl, A.A. Abou-Hussein, W. Linert, Syntheses, characterization, and biological activity of novel mono-and binuclear transition metal complexes with a hydrazone Schiff base derived from a coumarin derivative and oxalyldihydrazine, Monatshefte für Chemie-Chemical Monthly 149(2) (2018) 431-443.
[45] K. Al-Adilee, H.A. Kyhoiesh, Preparation and identification of some metal complexes with new heterocyclic azo dye ligand 2-[2−-(1-Hydroxy-4-Chloro phenyl) azo]-imidazole and their spectral and thermal studies, Journal of Molecular Structure 1137 (2017) 160-178.
[46] K.J. AL-Adilee, A.K. Abass, A.M. Taher, Synthesis of some transition metal complexes with new heterocyclic thiazolyl azo dye and their uses as sensitizers in photo reactions, Journal of Molecular Structure 1108 (2016) 378-397.
[47] P. Gull, M.A. Malik, O.A. Dar, A.A. Hashmi, Design, synthesis and spectroscopic characterization of metal (II) complexes derived from a tetradentate macrocyclic ligand: Study on antimicrobial and antioxidant capacity of complexes, Microbial pathogenesis 104 (2017) 212-216.
[48] P.A. Asbell, S.P. Epstein, J.A. Wallace, D. Epstein, C.C. Stewart, R.M. Burger, Efficacy of cobalt chelates in the rabbit eye model for epithelial herpetic keratitis, Cornea 17(5) (1998) 550-557.
[49] P.S. Deshmukh, A. Yaul, J.N. Bhojane, A. Aswar, Synthesis, characterization and thermogravimetric studies of some metal complexes with N 2 O 2 Schiff base ligand, World Appl. Sci. J 9 (2010) 1301-1305.
[50] S. Kundu, S. Maity, T. Weyhermüller, P. Ghosh, Oxidovanadium catechol complexes: Radical versus non-radical states and redox series, Inorganic chemistry 52(13) (2013) 7417-7430.
[51] G. Nahari, L. Reytman, L. Vendier, E.Y. Tshuva, C. Lorber, Cytotoxic Vanadium Complexes of Branched [ONNO]-Type Diamine Bis (phenolato) Ligands, European Journal of Inorganic Chemistry 2017(12) (2017) 1807-1811.